



Article

Unique Regulation of Intestinal Villus Epithelial $\text{Cl}^-/\text{HCO}_3^-$ Exchange by Cyclooxygenase Pathway Metabolites of Arachidonic Acid in a Mouse Model of Spontaneous Ileitis

M Motiur Rahman, Alip Borthakur , Sheuli Afroz, Subha Arthur and Uma Sundaram *

Department of Clinical and Translational Sciences, Joan C. Edwards School of Medicine, Marshall University, Huntington, WV 25701, USA; rahmanmd@marshall.edu (M.M.R.); borthakur@marshall.edu (A.B.); afroz@marshall.edu (S.A.); arthursu@marshall.edu (S.A.)

* Correspondence: sundaramu@marshall.edu; Tel.: +1-304-691-1841

Abstract: Electrolytes (NaCl) and fluid malabsorption cause diarrhea in inflammatory bowel disease (IBD). Coupled NaCl absorption, mediated by Na^+/H^+ and $\text{Cl}^-/\text{HCO}_3^-$ exchanges on the intestinal villus cells brush border membrane (BBM), is inhibited in IBD. Arachidonic acid metabolites (AAMs) formed via cyclooxygenase (COX) or lipoxygenase (LOX) pathways are elevated in IBD. However, their effects on NaCl absorption are not known. We treated SAMP1/YitFc (SAMP1) mice, a model of spontaneous ileitis resembling human IBD, with Arachidonyl Trifluoro Methylketone (ATMK, AAM inhibitor), or with piroxicam or MK-886, to inhibit COX or LOX pathways, respectively. $\text{Cl}^-/\text{HCO}_3^-$ exchange, measured as DIDS-sensitive ^{36}Cl uptake, was significantly inhibited in villus cells and BBM vesicles of SAMP1 mice compared to AKR/J controls, an effect reversed by ATMK. Piroxicam, but not MK-886, also reversed the inhibition. Kinetic studies showed that inhibition was secondary to altered K_m with no effects on V_{max} . Whole cell or BBM protein levels of Down-Regulated in Adenoma (SLC26A3) and putative anion transporter-1 (SLC26A6), the two key BBM $\text{Cl}^-/\text{HCO}_3^-$ exchangers, were unaltered. Thus, inhibition of villus cell $\text{Cl}^-/\text{HCO}_3^-$ exchange by COX pathway AAMs, such as prostaglandins, via reducing the affinity of the exchanger for Cl^- , and thereby causing NaCl malabsorption, could significantly contribute to IBD-associated diarrhea.

Keywords: $\text{Cl}^-/\text{HCO}_3^-$ exchange; COX pathway; inflammation; prostaglandins; SAMP1 mice



Citation: Rahman, M.M.; Borthakur, A.; Afroz, S.; Arthur, S.; Sundaram, U. Unique Regulation of Intestinal Villus Epithelial $\text{Cl}^-/\text{HCO}_3^-$ Exchange by Cyclooxygenase Pathway Metabolites of Arachidonic Acid in a Mouse Model of Spontaneous Ileitis. *Int. J. Mol. Sci.* **2021**, *22*, 4171. <https://doi.org/10.3390/ijms22084171>

Academic Editor: Wade D. Van Horn

Received: 25 February 2021

Accepted: 13 April 2021

Published: 17 April 2021

Publisher's Note: MDPI stays neutral with regard to jurisdictional claims in published maps and institutional affiliations.



Copyright: © 2021 by the authors. Licensee MDPI, Basel, Switzerland. This article is an open access article distributed under the terms and conditions of the Creative Commons Attribution (CC BY) license (<https://creativecommons.org/licenses/by/4.0/>).

1. Introduction

Inflammatory Bowel Disease (IBD) is a chronic, relapsing, and remitting inflammatory disease of the gastrointestinal tract that encompasses both Crohn's disease (CD) and ulcerative colitis (UC) [1–3]. IBD affects more than 3.5 million people in the United States and Europe, with a steep increase in incidence over the past 50 years [4,5]. The etiology of IBD is complex, there is no cure, and the cause of the disease remains unclear, limiting the development of therapeutic strategy to prevent its occurrence. Therefore, the therapy is focused toward mitigation of symptoms, rather than cure of disease [1]. Diarrhea, the most common and disabling morbidity of human IBD, is prevalent in almost 80% of the patients [6]. IBD-associated diarrhea is multifactorial and appears to be the outcome of intricate pathophysiological events arising from widespread and sustained mucosal inflammation [6]. Akin to all diarrheal diseases, decreased absorption, increased secretion, or both, of fluid and electrolyte is a common manifestation of IBD-associated diarrhea [7–9]. However, the majority of the studies investigating its pathophysiology have suggested that the predominant mechanism of diarrhea in IBD involves impairment of electroneutral NaCl absorption, rather than altered anion secretion [10]. Electroneutral NaCl absorption in the mammalian small intestine occurs via a coupled mechanism of Na^+/H^+ exchange and $\text{Cl}^-/\text{HCO}_3^-$ exchange on the brush border membranes (BBMs) of absorptive villus cells. However, the vast majority of animal models of IBD used to study IBD-associated

diarrhea exhibit inflammation in the colon, with limited studies focused on electrolyte and fluid transport defects in Crohn's-like ileitis, most commonly occurring in the terminal ileum [1]. We have extensively used the rabbit model of chronic enteritis to investigate impaired nutrient transport in chronic small intestinal inflammation [11–15] and also demonstrated glucocorticoid reversal of the inhibition of $\text{Cl}^-/\text{HCO}_3^-$ exchange [16] and nitric oxide-mediated modulation of NaCl absorption [17].

In IBD, altered absorption of NaCl and water causing diarrhea could be mediated by inflammatory mediators known to be elevated in the inflamed intestine. Immune-inflammatory mediators such as the metabolites of arachidonic acid (AA) are known to infiltrate into the mucosa during intestinal inflammation. We and others have shown these metabolites to be increased in IBD patients and animal models of IBD [11,18,19]. Cytosolic phospholipase A2 (PLA2) catalyzes the release of AA from membrane phospholipids. In turn, the AA metabolites (AAMs) formed via cyclooxygenase (COX) or lipoxygenase (LOX) pathways may contribute to clinical diarrhea in IBD. Prostaglandins (PGs) and leukotrienes (LTs), the two major groups of AAM formed via the COX and the LOX pathways, respectively, have been implicated in the pathogenesis of a number of inflammatory diseases, including IBD [19]. We have previously shown in a rabbit model of chronic ileitis that prostaglandins, but not leukotrienes, alter NaCl absorption via inhibition of $\text{Cl}^-/\text{HCO}_3^-$ exchange in ileal villus cell BBM, but without having any effect on Na^+/H^+ exchange [20]. In the current study, we used SAMP1/YitFc (SAMP1) mice, which are models of spontaneous ileitis closely resembling human IBD, with AKR/J (AKR) as control to investigate the effects of chronic inflammation on NaCl absorption. Our results demonstrate significant inhibition of $\text{Cl}^-/\text{HCO}_3^-$ exchange in the BBM of ileal villus cells of SAMP1 mice compared to AKR/J mice. Further, inhibition of the formation of AAM in general, and the COX pathway AAM in particular, have reversed the inhibition of $\text{Cl}^-/\text{HCO}_3^-$ exchange in SAMP1 mice.

2. Results

2.1. Histologic Illustrations of Chronically Inflamed SAMP1 Mice and AKR Control Mice Ileum

Figure 1 shows the ileal cross sections from 10-week-old SAMP1 and AKR control mice stained with hematoxylin and eosin (H&E; magnification $\times 10$) staining. A normal structure in control AKR mice is shown as the typical long villi, short crypts and minimal intraepithelial immunocytes (Figure 1A). SAMP1 mice developed spontaneous, transmural inflammation of the terminal ileum characterized by discontinuous inflammatory infiltrates, crypt hypertrophy, villus blunting and distortion, and bowel wall thickening, resembling human IBD (Figure 1B). In vivo treatment of SAMP1 mice with piroxicam, a COX pathway inhibitor, did not show any morphological changes in SAMP1 mice, as shown in Figure 1C. Histologic results indicate that SAMP1 mice spontaneously develop lesions in their terminal ilea, reminiscent of human IBD, and in vivo treatment of SAMP1 mice with a COX pathway inhibitor has no effects on ileal structure.

2.2. Inhibition of $\text{Cl}^-/\text{HCO}_3^-$ Exchange Activity in BBMV Prepared from SAMP1 Mice Ileum

We have previously shown that Na^+/H^+ exchange is not altered in SAMP1 mice [21]. Since coupled NaCl absorption in the mammalian small intestine has been shown to be mediated by the dual operation of Na^+/H^+ and $\text{Cl}^-/\text{HCO}_3^-$, in this study, we studied $\text{Cl}^-/\text{HCO}_3^-$ exchange in villus cell BBMV of SAMP1 versus AKR mice. $\text{Cl}^-/\text{HCO}_3^-$ exchange activity, defined as HCO_3^- -dependent and DIDS-sensitive ^{36}Cl uptake, was present in the BBM of ileal villus cells from both AKR and SAMP1 mice. However, the results presented in Figure 2 show that $\text{Cl}^-/\text{HCO}_3^-$ exchange is significantly inhibited in SAMP1 BBMV compared to the AKR controls.

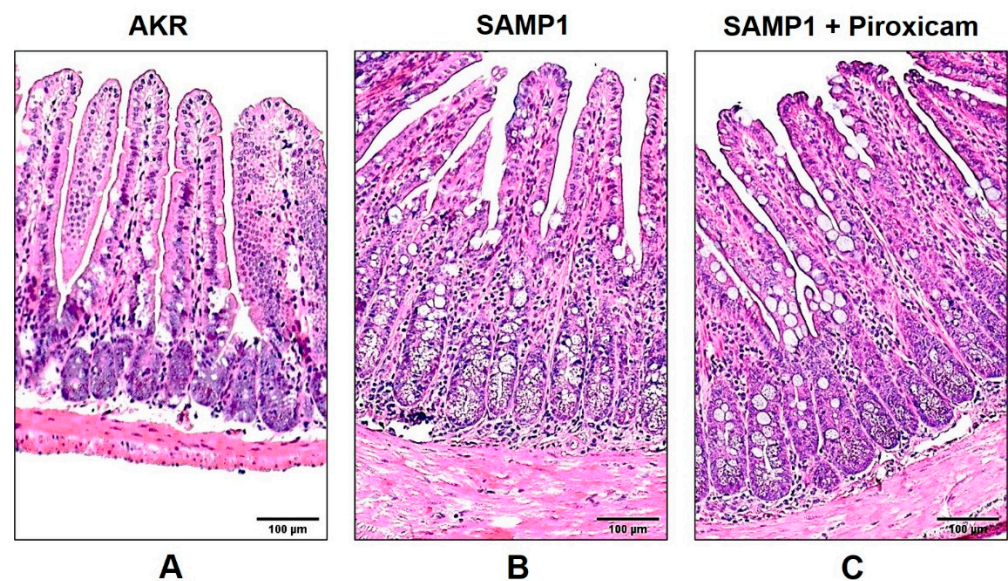


Figure 1. Illustrative photomicrographs of cross sections of the ileum of AKR and SAMP1 mice stained with hematoxylin and eosin (H&E). (A) The AKR mouse ileum depicts the typical long villi, short crypts and minimal intraepithelial immunocytes. (B) SAMP1 mouse intestine demonstrates crypt hypertrophy, villus blunting, and increased intraepithelial lymphocytes characteristic of inflammatory bowel disease (IBD). (C) In vivo treatment of SAMP1 mice with piroxicam, a COX pathway inhibitor, did not show any changes in the ileal structure in SAMP1 mice. Original magnification 10 \times . Scale bar 100 μ m.

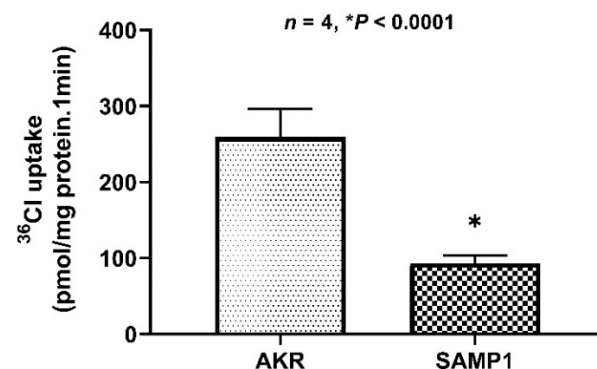


Figure 2. Inhibition of $\text{Cl}^-/\text{HCO}_3^-$ exchange activity in villus cell BBMVs of SAMP1 mice. $\text{Cl}^-/\text{HCO}_3^-$ exchange activity (^{36}Cl uptake, pmol/mg protein/min) was significantly inhibited in BBMVs prepared from ileal villus cells of SAMP1 mice compared to AKR controls. $N = 4$, * $p < 0.0001$.

2.3. Role of Arachidonic Acid Metabolites (AAMs) in Inhibiting $\text{Cl}^-/\text{HCO}_3^-$ Exchange in SAMP1 Mice

Soluble mediators generated in response to immune activation play important roles in mucosal inflammation in IBD [19]. The AAMs, including prostaglandins, comprise an important group of soluble mediators elevated in IBD and exert multiple effects [19]. AAMs have been shown to stimulate Cl^- secretion [22]; however, their effects on Cl^- absorption are not known. Therefore, we used Arachidonyl Trifluoro Methylketone (ATMK), an inhibitor of AAM formation, to treat SAMP1 and AKR mice intraperitoneally (3 mg/kg) for 2 days. Next, $\text{Cl}^-/\text{HCO}_3^-$ exchange activity was measured in ileal villus cell BBMVs from SAMP1 and AKR mice. As shown in Figure 3, $\text{Cl}^-/\text{HCO}_3^-$ exchange was significantly increased in response to ATMK treatment in SAMP1 mice (upper panel), whereas in AKR controls, ATMK showed no effect on $\text{Cl}^-/\text{HCO}_3^-$ exchange (lower panel). These results suggest that inhibition of $\text{Cl}^-/\text{HCO}_3^-$ exchange in SAMP1 mice could be mediated by AAM generated in the inflamed mucosa.

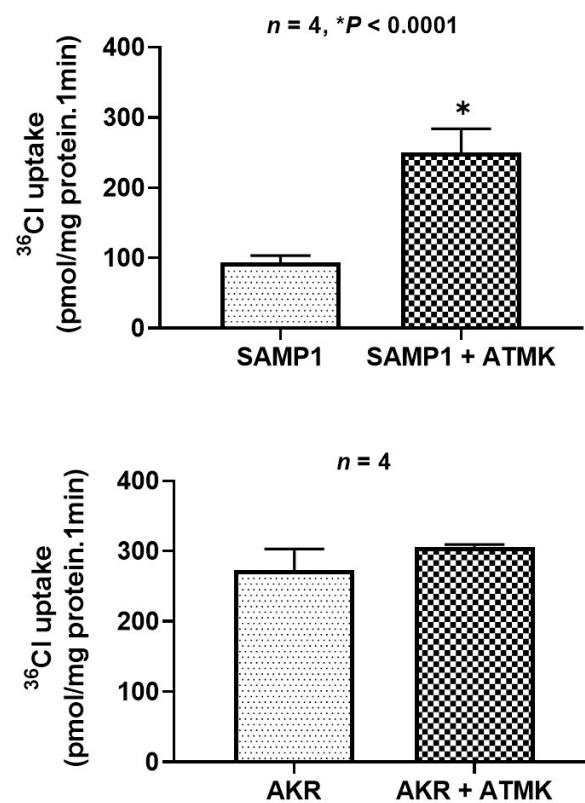


Figure 3. ATMK treatment of SAMP1 mice reversed the inhibition of $\text{Cl}^-/\text{HCO}_3^-$ exchange activity. Mice were treated intraperitoneally with ATMK (3 mg/kg), inhibitor of AAM formation, for 2 days. $\text{Cl}^-/\text{HCO}_3^-$ exchange activity was measured in ileal villus cell BBMVs. ATMK treatment stimulated $\text{Cl}^-/\text{HCO}_3^-$ exchange in SAMP1 mice compared to untreated mice (upper panel) $n = 4, *p < 0.0001$; in AKR mice, ATMK had no effect on $\text{Cl}^-/\text{HCO}_3^-$ exchange (lower panel).

2.4. Cyclooxygenase (COX) but Not Lipoxygenase (LOX) Pathway Metabolites of AA Inhibit $\text{Cl}^-/\text{HCO}_3^-$ Exchange in SAMP1 Mice

Major pathways of AA metabolism relevant to IBD are induced via activation of COX (COX-1, COX-2) and LOX (5-LOX, 12-LOX). To investigate which AAM, COX or LOX members are involved in inhibiting $\text{Cl}^-/\text{HCO}_3^-$ exchange, SAMP1 and AKR mice were treated intraperitoneally for 2 days with piroxicam (10 mg/kg) or MK-886 (0.5 mg/kg) to inhibit COX or LOX pathways of AAM formation, respectively, and then, $\text{Cl}^-/\text{HCO}_3^-$ exchange activities were measured in BBMVs. Results presented in Figure 4 show that piroxicam treatment diminished the inhibition of $\text{Cl}^-/\text{HCO}_3^-$ exchange in SAMP1 mice (4A, upper panel) but had no effect on $\text{Cl}^-/\text{HCO}_3^-$ exchange in AKR mice (4A, lower panel). On the other hand, MK-886, while showing no effect on $\text{Cl}^-/\text{HCO}_3^-$ exchange in AKR mice (4B, upper panel), did not block the inhibition of $\text{Cl}^-/\text{HCO}_3^-$ exchange in SAMP1 mice (4B, lower panel). These results suggest that in SAMP1 mice, inhibition of $\text{Cl}^-/\text{HCO}_3^-$ exchange is mediated by the COX pathway metabolites of AA, not by the LOX pathway AAMs.

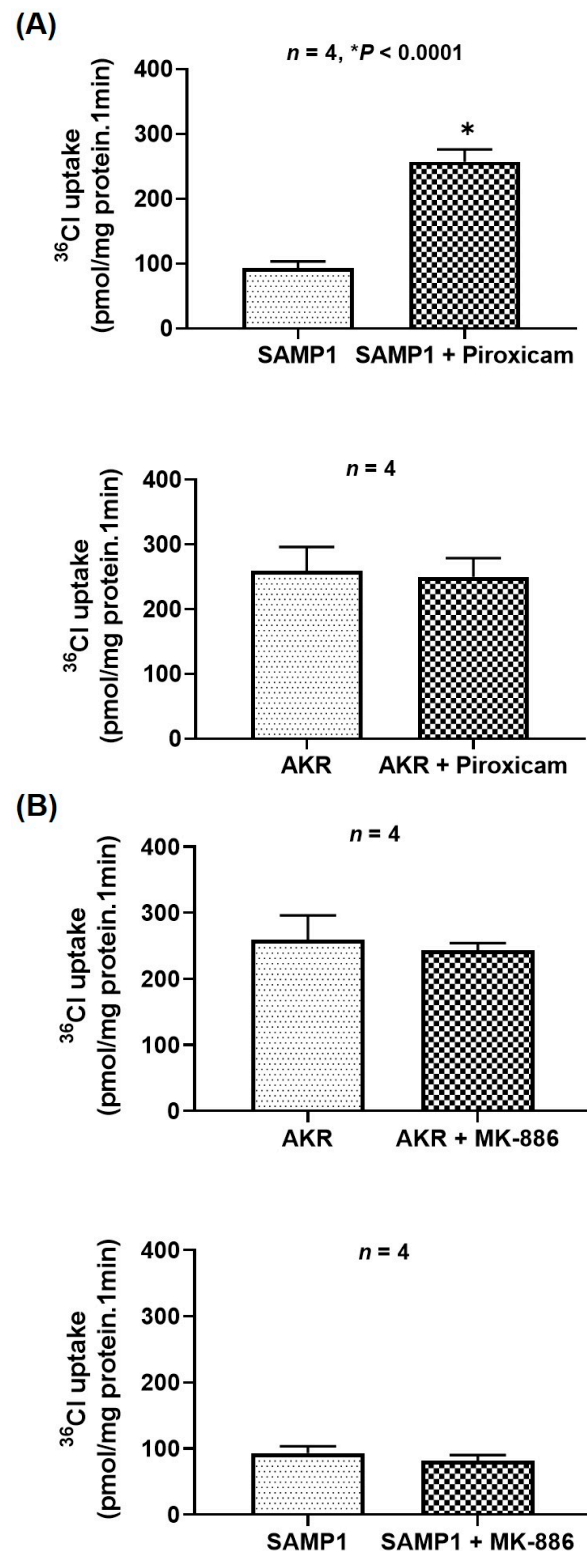


Figure 4. Effect of (A) piroxicam or (B) MK-886 treatment on $\text{Cl}^-/\text{HCO}_3^-$ exchange activity in SAMP1 mice. Mice were treated intraperitoneally for 2 days with piroxicam (10 mg/kg) or MK-886 (0.5 mg/kg) to inhibit COX or LOX pathways of AAM formation, respectively, and then, $\text{Cl}^-/\text{HCO}_3^-$ exchange activities were measured in BBMVs. (A) Piroxicam treatment significantly stimulated $\text{Cl}^-/\text{HCO}_3^-$ exchange in SAMP1 mice (upper panel) ($n = 4$, $* p < 0.0001$), but had no effect in AKR mice (lower panel). (B) MK-886, while showing no effect on $\text{Cl}^-/\text{HCO}_3^-$ exchange in AKR mice (upper panel), did not block the inhibition of $\text{Cl}^-/\text{HCO}_3^-$ exchange in SAMP1 mice (lower panel).

2.5. Kinetic Analysis of AAM-Mediated Inhibition of $\text{Cl}^-/\text{HCO}_3^-$ Exchange in SAMP1 Mice

Kinetic studies were performed to determine the mechanism of inhibition of $\text{Cl}^-/\text{HCO}_3^-$ exchange by AAM by measuring $\text{Cl}^-/\text{HCO}_3^-$ exchange activity in ileal villus cells from SAMP1/AKR at increasing concentrations (0.5–50 mM) of the substrate (Cl^-). In the villus cells from SAMP1 mice, the affinity of the $\text{Cl}^-/\text{HCO}_3^-$ exchanger protein for Cl^- was decreased, as compared to AKR villus cells, as represented by an increase in K_m . Treatment of SAMP1 mice with piroxicam reversed this effect, restoring the K_m value comparable to AKR control (Table 1, Figure 5). These results suggest that the mechanism of inhibition of $\text{Cl}^-/\text{HCO}_3^-$ exchange in SAMP1 mice villus cells was secondary to a decrease in the affinity of the exchanger ($1/K_m$) for Cl^- , rather than a reduction in the exchanger number, as the maximal rate of uptake by the exchanger (V_{\max}) was not altered.

Table 1. Kinetic parameters for $\text{Cl}^-/\text{HCO}_3^-$ exchange. The affinity ($1/K_m$) of $\text{Cl}^-/\text{HCO}_3^-$ exchanger for substrate (Cl^-) was significantly decreased in the villus cells from SAMP1 mice compared to the control. The decrease in affinity was completely restored to normal in the villus cells obtained from piroxicam-treated SAMP1 mice.

	V_{\max} (nmol/mg Protein/min)	K_m (mM)
AKR	1.60 ± 0.02	10.81 ± 0.26
SAMP1	1.65 ± 0.05	18.84 ± 0.76
SAMP1 + Piroxicam	1.66 ± 0.04	11.83 ± 0.48

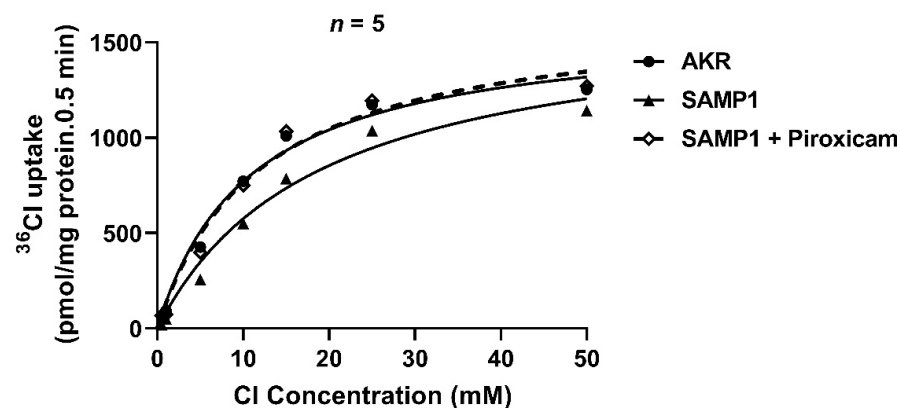


Figure 5. Kinetics of $\text{Cl}^-/\text{HCO}_3^-$ exchange in villus cells from AKR, SAMP1, and piroxicam-treated SAMP1 mice. DIDS-sensitive ^{36}Cl uptake in different groups is shown as a function of varying concentrations of extracellular Cl^- . Analysis of the kinetic parameters (K_m and V_{\max}) by GraphPad Prism software showed no significant alteration of V_{\max} in all the groups. In SAMP1 mice, there was a significant increase in K_m (decrease in $1/K_m$) ($n = 5$) compared to AKR mice. Piroxicam treatment restored the K_m to normal, comparable to that of AKR mice.

2.6. Protein Levels of the BBM $\text{Cl}^-/\text{HCO}_3^-$ Exchangers Are Not Altered in SAMP1 Mice

In the mammalian intestine, the two key BBM $\text{Cl}^-/\text{HCO}_3^-$ exchanger proteins of the SLC26 family, Down-Regulated in Adenoma (DRA, SLC26A3) and putative anion transporter-1 (PAT1, SLC26A6), mediate Cl^- absorption. The kinetic studies (Table 1, Figure 5) suggested that inhibition of $\text{Cl}^-/\text{HCO}_3^-$ exchange in SAMP1 mice villus cells was secondary to a decrease in the affinity of the exchanger ($1/K_m$) for Cl^- , rather than a reduction in the exchanger number. Therefore, protein levels of the exchangers DRA and PAT1 were measured in the lysates of intact villus cells and in the BBM for all groups of mice. As shown in Figure 6, protein levels of DRA and PAT1 in the BBM (6A) or whole cell lysates (6B) were not altered in any of the groups (AKR, SAMP1, ATMK, piroxicam), further supporting our kinetics data that inhibition of $\text{Cl}^-/\text{HCO}_3^-$ exchange in SAMP1 mice was not secondary to decreased number of exchangers.

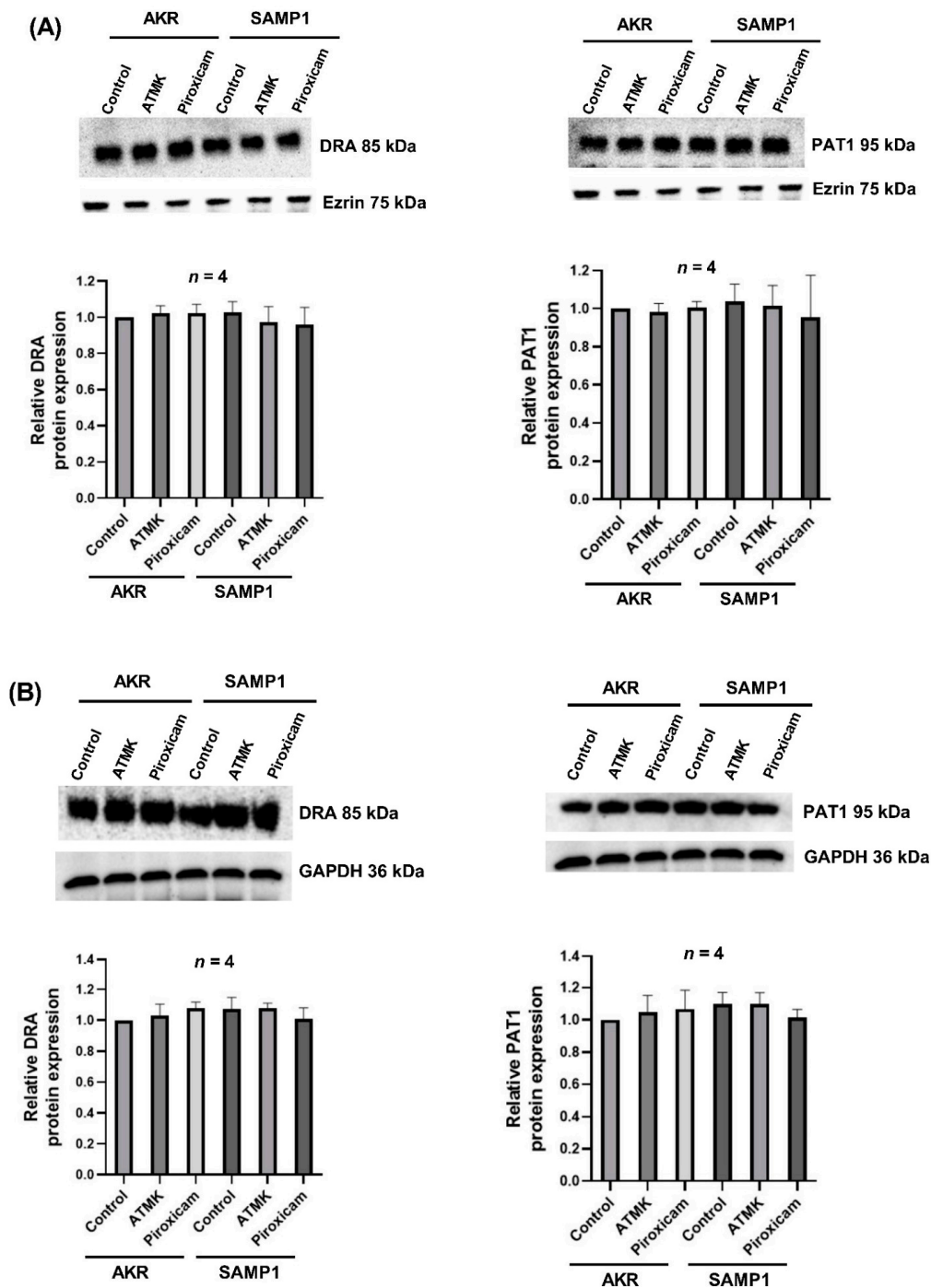


Figure 6. Protein levels of the BBM $\text{Cl}^-/\text{HCO}_3^-$ exchangers (DRA and PAT1) are not altered in SAMP1 mice. Protein samples prepared from (A) BBM or (B) cellular homogenate protein preparations from AKR and SAMP1. SAMP1 treated with ATMK or piroxicam was loaded (50 $\mu\text{g}/\text{sample}$) and separated on a 10% SDS-polyacrylamide gel, transferred onto a PVDF membrane, and probed with anti-DRA or anti-PAT1 antibodies as described in the Materials and Methods. Ezrin and GAPDH were used as the internal control. In both (A,B), a representative blot of 4 independent experiments (upper panels) and densitometric analyses of band intensities (lower panels) are shown. There were no alterations in the levels of DRA or PAT1 proteins in all groups.

2.7. Immunostaining of Mucosal DRA and PAT1 in SAMP1 Small Intestine

To further confirm the mechanism of inhibition of $\text{Cl}^-/\text{HCO}_3^-$ exchangers (DRA, PAT1) in SAMP1 mice, immunofluorescence studies were performed. Images were captured at 20 \times magnification. The levels of DRA protein in the BBM of villus cells was similar in

AKR and SAMP1 mice and piroxicam treatment had no effect on DRA in either AKR or SAMP1 mice (Figure 7A). Similarly, levels of PAT1 protein in the BBM of villus cells were unaltered in AKR and SAMP1 mice or in response to piroxicam treatment (Figure 7B). The combined results of kinetic studies, Western blot and immunohistochemical studies clearly suggest that the inhibition of $\text{Cl}^-/\text{HCO}_3^-$ exchange, mediated by DRA and/or PAT1, is secondary to altered affinity of the exchanger for Cl^- .

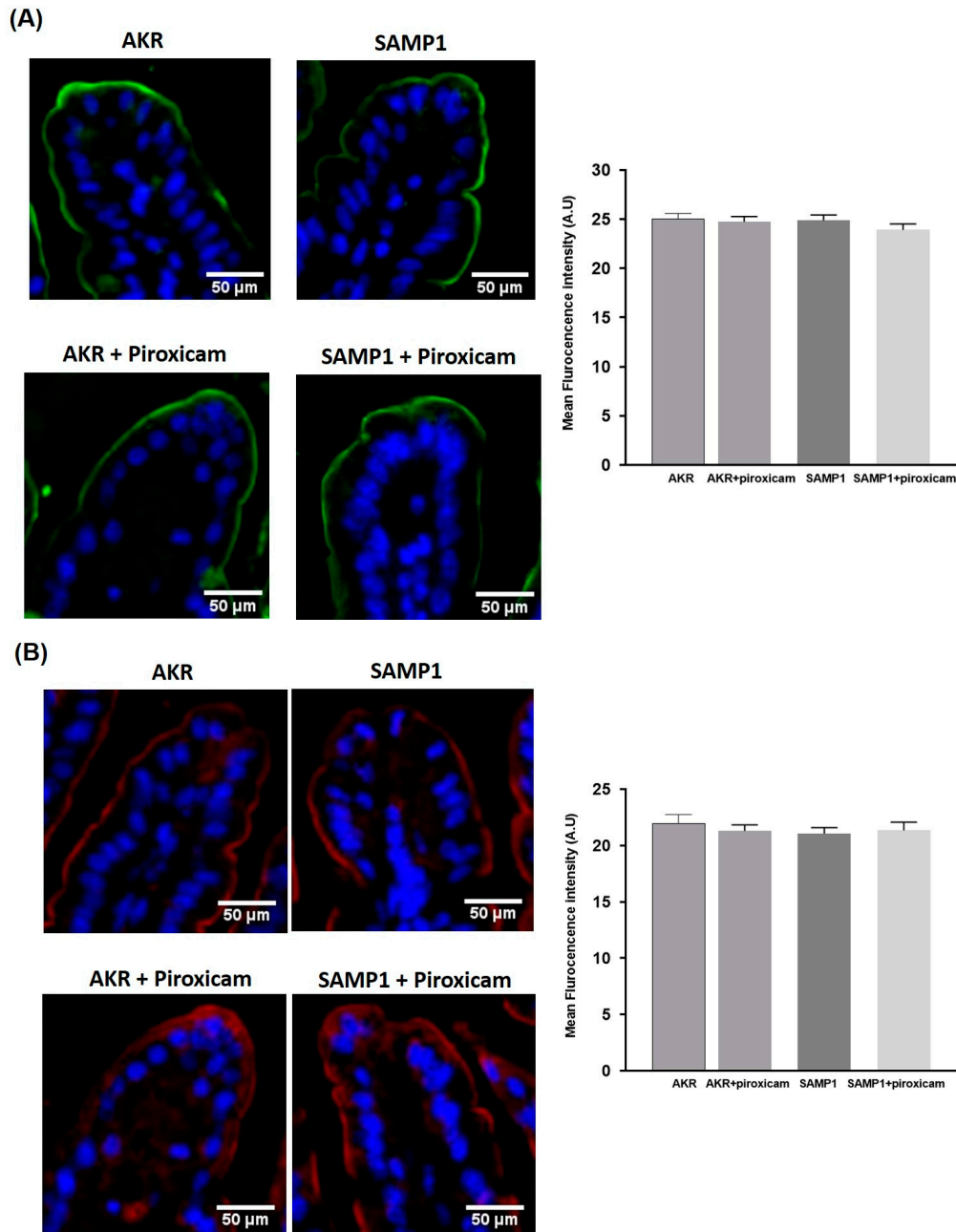


Figure 7. Immunofluorescence staining of DRA and PAT1 in small intestinal mucosa of SAMP1/AKR mice. (A) (Left panel): Immunofluorescence staining of small intestinal mucosal sections of AKR and SAMP1 mice for DRA (green) and DAPI (blue). Representative image of 4 independent experiments is shown. Images were captured at 20× magnification. (Right panel): Quantification of DRA immunostaining intensity by Image J software showed no alterations of DRA levels in AKR versus SAMP1 mice or in response to piroxicam treatments. (B) (Left panel): Immunofluorescence staining of small intestinal mucosal sections of AKR and SAMP1 mice for PAT1 (red) and DAPI (blue). Representative image of 4 independent experiments is shown. (Right panel): Quantification of DRA immunostaining intensity by Image J software showed no alterations of PAT1 protein levels in AKR versus SAMP1 mice or in response to piroxicam treatments.

3. Discussion

In the current study, we used SAMP1/YitFc (SAMP1) mice, a model of spontaneous ileitis closely resembling human inflammatory bowel disease (IBD), to investigate the impact of chronic inflammation on NaCl absorption. Our results demonstrated significant inhibition of $\text{Cl}^-/\text{HCO}_3^-$ exchange, a component of coupled NaCl absorption in the brush border membrane (BBM) of intestinal villus cells in chronic inflammation. Chronic, recurring, and bloody diarrhea is a common and disabling morbidity of inflammatory bowel disease (IBD), a debilitating inflammatory disease of the intestine. Dysregulated fluid and ion transport is a hallmark of most diarrheal diseases [23,24]. In IBD, activation of the immune system results in the production of soluble mediators by the immune cells, causing mucosal injury and chronic inflammation. In the inflamed mucosa, normal fluid and electrolyte (NaCl) transport, absorption and/or secretion across the epithelium are disturbed. Extensive studies focused on the molecular pathophysiology of IBD-associated diarrhea, however, suggest that impaired NaCl absorption, rather than anion secretion, primarily contributes to diarrhea in IBD [10]. The major route of NaCl absorption in the intestine is via a coupled electroneutral mechanism of Na^+/H^+ exchange and $\text{Cl}^-/\text{HCO}_3^-$ exchange mediated by Na^+/H^+ exchanger 3 (NHE3, SLC9A3) and Down-Regulated in Adenoma (DRA, SLC26A3), respectively [25,26]. NHE2 and SLC26A6 (PAT1) expressed on the apical surface also mediate Na^+/H^+ and $\text{Cl}^-/\text{HCO}_3^-$ exchange, respectively [25,26]. In a rabbit model of chronic intestinal inflammation, in many aspects resembling human IBD, we have previously shown unique mechanisms of alteration of nutrient absorption [11–15]. Indeed, in the same model, we have also shown glucocorticoid-mediated reversal of the inhibition of the inhibition of $\text{Cl}^-/\text{HCO}_3^-$ exchange [16] and nitric oxide-mediated modulation of NaCl absorption [17].

Most of the studies reported so far on impaired NaCl absorption in IBD utilized animal models of acute or chronic inflammation of the colon, with limited studies performed in models of small intestinal inflammation that manifest Crohn's disease, most commonly occurring in the terminal ileum [1]. In the current study, we used SAMP1/YitFc mice, a model of spontaneous ileitis closely resembling small intestinal inflammation in human IBD, to investigate the mechanisms of alteration of NaCl absorption. SAMP1/YitFc inbred mouse strain, which develops ileitis spontaneously, without chemical, genetic, or immunologic manipulation, is highly relevant to Crohn's-like ileitis [1]. In this model, for the first time, we previously reported the role of inducible nitric oxide (iNO) in inhibiting $\text{Cl}^-/\text{HCO}_3^-$ exchange in the brush border membrane (BBM) of ileal villus cells with no alteration of Na^+/H^+ exchange [27]. In the current study, we have investigated the mechanism of inhibition of $\text{Cl}^-/\text{HCO}_3^-$ exchange and demonstrated the role of arachidonic acid metabolites (AAMs), known to be elevated in the inflamed mucosa, in mediating inhibition of $\text{Cl}^-/\text{HCO}_3^-$ exchange. Akin to our previous report [27], there was significant inhibition of $\text{Cl}^-/\text{HCO}_3^-$ exchange in villus cells and BBMV prepared from villus cells of SAMP1 mice as compared to the AKR controls. When these mice were treated with ATMK to inhibit AAM formation, inhibition of $\text{Cl}^-/\text{HCO}_3^-$ exchange in SAMP1 mice was abrogated, with no effect in AKR mice.

In most cells, arachidonic acid (AA) is present primarily as a component of plasma membrane phospholipids. Activation of phospholipases, particularly phospholipase A2 (PLA2), by various cellular or extracellular factors releases AA from phospholipids. Major pathways of AA metabolism relevant to IBD include cyclooxygenase (COX) and lipoxygenase (LOX) [19]. Therefore, we used inhibitors of COX and LOX pathways to treat SAMP1/AKR mice to ascertain which pathway AAM could inhibit $\text{Cl}^-/\text{HCO}_3^-$ exchange in chronic inflammation. Our results showed that inhibition of COX pathway, but not LOX pathway of AAM formation, reversed the inhibition of $\text{Cl}^-/\text{HCO}_3^-$ exchange in SAMP1 mice. These inhibitors, as expected, had no effects on $\text{Cl}^-/\text{HCO}_3^-$ exchange in AKR mice. These results clearly suggest the role of prostaglandins, key AAMs formed via the COX pathway, in inhibiting $\text{Cl}^-/\text{HCO}_3^-$ exchange in SAMP1 mice. These findings are also consistent with our earlier demonstration that prostaglandins, but not leukotrienes

(LOX pathway AAM) regulate $\text{Cl}^-/\text{HCO}_3^-$ exchange in villus cells of chronically inflamed rabbit ileum, further supporting the impact of elevated AAM, more specifically of the prostaglandins, on NaCl absorption in IBD [20]. Our kinetic studies further showed that AAM-mediated inhibition of $\text{Cl}^-/\text{HCO}_3^-$ exchange in SAMP1 mice is secondary to the reduction in the affinity of the exchanger protein for Cl^- , not due to an altered exchanger number. That there was no alteration of exchanger number was further addressed by measuring the total cellular and BBM levels of DRA and PAT1, the key $\text{Cl}^-/\text{HCO}_3^-$ exchanger proteins in the mammalian intestinal BBM. Protein levels of DRA and PAT1 in the villus cells or in the purified BBM were similar in SAMP1 and AKR mice, which also did not change in response to any of the treatments.

Affinity of the SLC transporters for their respective substrates could be altered via post-translational modifications of the transporter proteins that commonly occur via addition of a functional group, such as phosphorylation and glycosylation [28]. Prostaglandins induce various signaling pathways via activation of their G-protein coupled receptors. In intestinal epithelial cells, EP2 and EP4, receptors for PGE₂, a key prostaglandin formed from AA, are highly expressed [21]. Both EP2 and EP4 are coupled to G α s proteins; therefore, upon activation, increase intracellular cyclic AMP (cAMP) via activation of adenylyl cyclase and in turn activate various downstream kinases. Therefore, future studies are needed to elucidate the role of phosphorylation and/or other likely post-translational modification of DRA and/or PAT1 in AAM-mediated inhibition of $\text{Cl}^-/\text{HCO}_3^-$ exchange in SAMP1 mice.

In the current study, as well as in our previous studies in a rabbit model of ileitis [20], $\text{Cl}^-/\text{HCO}_3^-$ exchange in the villus cell BBM was found to be inhibited by prostaglandins, but there was no effect on the Na^+/H^+ exchange, a process known to be commonly coupled to $\text{Cl}^-/\text{HCO}_3^-$ exchange in the mammalian intestine. In addition to this major pathway of electroneutral NaCl absorption, there are pathways of nutrient-dependent absorption of Na^+ , mediated by Na^+ -glucose/amino acid symporters in the villus cell BBM [3]. In this regard, Na^+ /glucose cotransport mediated by BBM SGLT1 not only represents the unequivocal pathway for the absorption of the major nutrient glucose, but also plays a critical role in maintaining overall fluid and electrolyte homeostasis [29]. Indeed, Na^+ -glucose co-transport is the basis of Oral Rehydration Solution (ORS), used to treat dehydration due to diarrhea [30–32]. It seems quite logical to speculate that in IBD Na^+ /glucose cotransport and/or other Na^+ /nutrient symport mechanisms could have greater relevance to account for impaired NaCl absorption, which is further supported by the fact that the absorption of both electrolytes and nutrients (such as glucose) is substantially inhibited in this chronic inflammatory disease [33]. Therefore, it will be important in future studies to investigate the impact of elevated levels of AAM on Na^+ /glucose cotransport and/or other Na^+ /nutrient symport processes in the pathophysiology of IBD-associated diarrhea.

In summary, the current study demonstrates that metabolites of arachidonic acid generated via COX pathway inhibit $\text{Cl}^-/\text{HCO}_3^-$ exchange by decreasing the affinity of the exchanger protein for Cl^- . Since prostaglandins, COX pathway AAMs, are known to be elevated in IBD, modulation of NaCl absorption by prostaglandins appears to be a significant factor contributing to IBD-associated diarrhea.

4. Materials and Methods

4.1. Chemicals and Antibodies

Arachidonyl Trifluoro Methylketone (ATMK), piroxicam and MK-886 were purchased from Cayman Chemical Company (Ann Arbor, MI, USA). Anti-DRA antibody raised in goat (sc-34939) and anti-PAT1 antibody raised in goat (sc-26728) were obtained from Santa Cruz Biotechnology (Dallas, TX, USA).

4.2. Mouse Model of Chronic Ileitis

Male SAMP1/YitFc (SAMP1) and age matched control AKR/J (AKR) male mice obtained from Jackson Laboratory (Farmington, CT, USA) were maintained in a 12 h light/dark cycle with free access to food and water in the Animal Care Facility at Byrd

Biotechnology Science Center, Marshall University. After a week of acclimatization, the animals were included in the study at 10 weeks of age. SAMP1 and AKR mice were treated intraperitoneally for 2 days with ATMK (3 mg/kg), or with piroxicam (10 mg/kg) or MK-886 (0.5 mg/kg) and were euthanized at the end of the second day of treatment with excess carbon dioxide exposure. All the animal studies described in the manuscript were carried out strictly in accordance with the procedural and ethical regulations of Marshall University's Institutional Animal Care and Use Committee (IACUC approval number 743, Approval date 17th May 2020).

4.3. Isolation of Villus Cells

Villus cells from the scrapped small intestinal mucosa of the animals were isolated by a calcium chelation technique as previously described by us [34,35]. Briefly, the distal small intestine extracted from these mice were filled with cell isolation buffer (0.15 mM EDTA, 112 mM NaCl, 25 mM NaHCO₃, 2.4 mM K₂HPO₄, 0.4 mM KH₂PO₄, 2. mM l-glutamine, 0.5 mM β-hydroxybutyrate, and 0.5 mM dithiothreitol; gassed with 95% O₂ and 5% CO₂; pH 7.4) and incubated in 37 °C water bath for 3 min, followed by gentle palpitation for another 3 min to facilitate cell separation. The isolation buffer with the isolated villus cells was then drained from the intestine and centrifuged at 100× g for 3 min. The cell pellet thus obtained was flash frozen immediately in liquid nitrogen and stored at −80 °C until experimental use.

4.4. Preparation of Brush Border Membrane Vesicles (BBMVs)

Ileal villus BBM vesicles (BBMVs) from mice were prepared by Mg⁺⁺ precipitation and differential centrifugation [36,37].

4.5. Measurement of Cl[−]/HCO₃[−] Exchange Activity

Cl[−]/HCO₃[−] exchange activity was measured in BBMVs by rapid-filtration technique as previously described [17,20]. BBMVs were suspended in vesicle medium and either 50 mM KHCO₃ (vesicle gassed with 5% CO₂ and 95% N₂) or 50 mM potassium gluconate (vesicle gassed with 100% N₂). The reaction was started by adding 5 μL of vesicle to 95 μL reaction mixture with or without 1 mM 4,4-diisothiocyanatostilbene-2,2-disulfonic acid disodium salt (DIDS), a potent anion exchange inhibitor [17,20]. The uptake was stopped at 60 s with ice-cold stop solution containing 50 mM HEPES-Tris buffer (pH 7.5), 0.10 mM MgSO₄, 50 mM potassium gluconate and 100 mM N-methyl-d-glucamine (NMG) gluconate [17,20]. Each reaction mixture was then filtered on a 0.45 μm Millipore (HAWP) filter and washed twice with 5 mL of the ice-cold stop solution. The filter was then dissolved in 5 mL scintillation fluid (Ecoscint, National Diagnostics), and radioactivity was determined in a Perkin Elmer Tri-Carb LSC 4910TR Scintillation Counter. The uptake numbers were calculated as HCO₃[−]-dependent DIDS-sensitive ³⁶Cl[−] uptake to determine Cl[−]/HCO₃[−] exchange activity.

4.6. Kinetic Studies

To determine the kinetic parameters, Cl[−]/HCO₃[−] exchange activity was measured in intact villus cells isolated from AKR mice and SAMP1 mice treated or untreated with ATMK for 2 days. The isolated cells (100 mg) were suspended in buffers containing 5 mM NMG gluconate and 50 mM HEPES-Tris (pH 7.5) with 100 mM KHCO₃ or 100 mM K-gluconate. The uptake reaction was started by adding the suspended cells to a reaction mixture containing 5 mM NMG ³⁶Cl[−], 150 mM potassium gluconate, 50 mM MES-Tris (pH 5.5) and varying concentrations of HCl (0.5, 1, 5, 15, 25 and 50 mM) with or without 1 mM DIDS. The uptake was stopped at 30 s with the addition of an ice-cold stop solution containing 50 mM HEPES-Tris buffer (pH 7.5), 0.10 mM MgSO₄, 50 mM potassium gluconate and 100 mM NMG gluconate. Each reaction mixture was then filtered on a 0.65 μm Millipore (DAWP) filter and washed twice with 5 mL of the ice-cold stop solution. The filter was then dissolved in 5 mL scintillation fluid (Ecoscint, National Diagnostics) and radioactivity

was determined as described above. Uptake numbers that were obtained from these experiments were analyzed with GraphPad Prism 8 (GraphPad Software Inc., San Diego, CA, USA) for Michaelis–Menten kinetics using a nonlinear regression data analysis to derive kinetic parameters V_{\max} and K_m .

4.7. Western Blot

Homogenates of isolated villus cells were prepared by first centrifuging cells at $8000 \times g$ at 4°C for 5 min and solubilizing the resulting pellet in radioimmunoprecipitation (RIPA) buffer containing protease inhibitors (Santa Cruz). Cellular extracts in RIPA were then centrifuged at $8000 \times g$ at 4°C for 5 min, and the supernatant was measured for protein content with a NanoDrop Spectrophotometer (Thermo Scientific, Waltham, MA, USA). Proteins from BBM preparations were solubilized and extracted in RIPA buffer as above. Proteins were separated on 8% polyacrylamide gel, transferred onto a polyvinylidene difluoride membrane, blocked in 5% BSA for 1 h as previously described [38] and incubated with primary anti-DRA or anti-PAT1 antibodies at 4°C overnight. Horseradish peroxidase coupled specific secondary antibodies were used to bind to DRA and PAT1 bound primary antibodies before detecting chemiluminescence with ECL Detection Reagent (GE Healthcare, Chicago, IL, USA). The density of the DRA and PAT1 specific protein bands were quantitated with a densitometric scanner FluorChemTM instrument (Alpha Innotech, San Leandro, CA, USA) and normalized with ezrin (MAB3822-C, Millipore, Temecula, CA, USA) and GAPDH (MA5-15738, Thermo Fisher Scientific, Waltham, MA, USA) bands.

4.8. Histology and Immunohistochemistry

A portion of the distal ileum was tissue was fixed in 10% (*v/v*) neutral-buffered formalin (Sigma Aldrich, St Louis, MO, USA) and embedded in paraffin. Sections ($5\ \mu\text{m}$) from the formal fixed tissue were obtained with a microtome and were mounted on glass slides. Paraffin was removed from the sections by incubating the slides with xylene, and sections were hydrated gradually by incubating with graded ethanol. Sections were stained with hematoxylin and eosin (H&E; Sigma Aldrich, St Louis, MO, USA) staining. For the immunofluorescence study, antigen retrieval was performed by incubating the sections with 10 mM sodium citrate buffer, pH 6, at 95°C for 10 min as described previously (20). After washing with PBST (0.05% Tween-20 in phosphate buffered saline), sections were incubated in blocking buffer (2% bovine serum albumin) for 1 h at room temperature. The sections were then incubated for 1 h at room temperature with antichick DRA primary antibody (custom antibody services provided by Invitrogen Life Technologies), at 1:100 dilution and anti-PAT1 primary antibody (sc:515230, Santa Cruz Biotechnology, Inc. USA) at 1:100 dilution. Excess antibody was removed by washing with PBST and incubated with Alexa Fluor 488 goat antichick (A11039; Invitrogen Molecular Probes, Carlsbad, California) or Alexa Fluor 594 goat antimouse (A11032; Invitrogen Molecular Probes, Carlsbad, California) for DRA and PAT1, respectively, at 1:500 dilution for 1 h at room temperature. Sections were then washed thrice in PBST, and the nucleus was stained with 4, 9, 6-diamidino-2-phenylindole (DAPI) mount, i.e., Fluoroshield mounting medium with DAPI (ab104139, Abcam, USA) and observed with EVOS FL Cell imaging system. Images were quantified by using Image J software.

4.9. Statistical Analyses

Results are shown as means \pm standard error of mean (SEM). Statistical analysis (unpaired t test) was performed with GraphPad Prism 7 software to derive statistical significance between data derived from different experimental conditions. A *p* value of <0.05 was considered statistically significant. The *n* number for any set of experimental data refers to experiments performed with villus cells or BBMV preparations or protein extracts obtained from *n* different animals of each experimental group.

Author Contributions: M.M.R. and S.A. (Sheuli Afroz): methodology, experiment and data curation; A.B.: writing—original draft preparation; A.B., S.A. (Subha Arthur) and U.S.: writing—review and editing; U.S.: conceptualization and funding acquisition. All authors have read and agreed to the submitted version of the manuscript.

Funding: This work was supported by Veteran’s Administration Merit Review grant BX003443-01 and National Institutes of Health grants DK-67420, DK-108054, and P20GM121299-01A1 to US and AI130790-03 to AB.

Institutional Review Board Statement: All the animal studies described in the manuscript were carried out strictly in accordance with the procedural and ethical regulations of Marshall University’s Institutional Animal Care and Use Committee (IACUC approval number 743, Approval date May 17th 2020).

Informed Consent Statement: Not applicable.

Data Availability Statement: Not applicable.

Acknowledgments: The authors thank Usha Murughiyan for editorial assistance in the preparation of this manuscript.

Conflicts of Interest: All authors declare no conflicts of interest, financial or otherwise.

References

1. Cominelli, F.; Arseneau, K.O.; Rodriguez-Palacios, A.; Pizarro, T.T. Uncovering Pathogenic Mechanisms of Inflammatory Bowel Disease Using Mouse Models of Crohn’s Disease-Like Ileitis: What is the Right Model? *Cell Mol. Gastroenterol. Hepatol.* **2017**, *4*, 19–32. [[CrossRef](#)]
2. Longo, S.; Chieppa, M.; Cossa, L.G.; Spinelli, C.C.; Greco, M.; Maffia, M.; Giudetti, A.M. New Insights into Inflammatory Bowel Diseases from Proteomic and Lipidomic Studies. *Proteomes* **2020**, *8*, 18. [[CrossRef](#)]
3. Anbazhagan, A.N.; Priyamvada, S.; Alrefai, W.A.; Dudeja, P.K. Pathophysiology of IBD associated diarrhea. *Tissue Barriers* **2018**, *6*, e1463897. [[CrossRef](#)]
4. Kaplan, G.G. The global burden of IBD: From 2015 to 2025. *Nat. Rev. Gastroenterol. Hepatol.* **2015**, *12*, 720–727. [[CrossRef](#)] [[PubMed](#)]
5. Ananthakrishnan, A.N. Epidemiology and risk factors for IBD. *Nat. Rev. Gastroenterol. Hepatol.* **2015**, *12*, 205–217. [[CrossRef](#)]
6. Wenzl, H.H. Diarrhea in chronic inflammatory bowel diseases. *Gastroenterol. Clin. N. Am.* **2012**, *41*, 651–675. [[CrossRef](#)]
7. Magalhaes, D.; Cabral, J.M.; Soares-da-Silva, P.; Magro, F. Role of epithelial ion transports in inflammatory bowel disease. *Am. J. Physiol. Gastrointest. Liver Physiol.* **2016**, *310*, G460–G476. [[CrossRef](#)] [[PubMed](#)]
8. Seidler, U.; Lenzen, H.; Cinar, A.; Tessema, T.; Bleich, A.; Riederer, B. Molecular mechanisms of disturbed electrolyte transport in intestinal inflammation. *Ann. N. Y. Acad. Sci.* **2006**, *1072*, 262–275. [[CrossRef](#)] [[PubMed](#)]
9. Barkas, F.; Liberopoulos, E.; Kei, A.; Elisaf, M. Electrolyte and acid-base disorders in inflammatory bowel disease. *Ann. Gastroenterol.* **2013**, *26*, 23–28. [[PubMed](#)]
10. Priyamvada, S.; Gomes, R.; Gill, R.K.; Saksena, S.; Alrefai, W.A.; Dudeja, P.K. Mechanisms Underlying Dysregulation of Electrolyte Absorption in Inflammatory Bowel Disease-Associated Diarrhea. *Inflamm. Bowel Dis.* **2015**, *21*, 2926–2935. [[CrossRef](#)] [[PubMed](#)]
11. Sundaram, U.; Hassanain, H.; Suntres, Z.; Yu, J.G.; Cooke, H.J.; Guzman, J.; Christofi, F.L. Rabbit chronic ileitis leads to up-regulation of adenosine A1/A3 gene products, oxidative stress, and immune modulation. *Biochem. Pharmacol.* **2003**, *65*, 1529–1538. [[CrossRef](#)]
12. Singh, S.; Arthur, S.; Sundaram, U. Unique regulation of Na-glutamine cotransporter SN2/SNAT5 in rabbit intestinal crypt cells during chronic enteritis. *J. Cell Mol. Med.* **2018**, *22*, 1443–1451. [[CrossRef](#)]
13. Arthur, S.; Sundaram, U. Inducible nitric oxide regulates intestinal glutamine assimilation during chronic intestinal inflammation. *Nitric Oxide* **2015**, *44*, 98–104. [[CrossRef](#)]
14. Arthur, S.; Singh, S.; Sundaram, U. Cyclooxygenase pathway mediates the inhibition of Na-glutamine co-transporter B0AT1 in rabbit villus cells during chronic intestinal inflammation. *PLoS ONE* **2018**, *13*, e0203552. [[CrossRef](#)]
15. Sundaram, U.; Wisel, S.; Coon, S. Mechanism of inhibition of proton: Dipeptide co-transport during chronic enteritis in the mammalian small intestine. *Biochim. Biophys. Acta* **2005**, *1714*, 134–140. [[CrossRef](#)] [[PubMed](#)]
16. Coon, S.; Sundaram, U. Mechanism of glucocorticoid-mediated reversal of inhibition of Cl(-)/HCO(-)(3) exchange during chronic ileitis. *Am. J. Physiol. Gastrointest. Liver Physiol.* **2000**, *278*, G570–G577. [[CrossRef](#)]
17. Coon, S.; Sundaram, U. Unique regulation of anion/HCO3- exchangers by constitutive nitric oxide in rabbit small intestine. *Am. J. Physiol. Gastrointest. Liver Physiol.* **2003**, *285*, G1084–G1090. [[CrossRef](#)]
18. Nielsen, O.H.; Ahnfelt-Ronne, I.; Elmgreen, J. Abnormal metabolism of arachidonic acid in chronic inflammatory bowel disease: Enhanced release of leucotriene B4 from activated neutrophils. *Gut* **1987**, *28*, 181–185. [[CrossRef](#)]
19. Stenson, W.F. The universe of arachidonic acid metabolites in inflammatory bowel disease: Can we tell the good from the bad? *Curr. Opin. Gastroenterol.* **2014**, *30*, 347–351. [[CrossRef](#)] [[PubMed](#)]

20. Manoharan, P.; Coon, S.; Baseler, W.; Sundaram, S.; Kekuda, R.; Sundaram, U. Prostaglandins, not the leukotrienes, regulate Cl⁻/HCO₃⁻ exchange (DRA, SLC26A3) in villus cells in the chronically inflamed rabbit ileum. *Biochim. Biophys. Acta* **2013**, *1828*, 179–186. [[CrossRef](#)] [[PubMed](#)]
21. Olsen Hult, L.T.; Kleiveland, C.R.; Fosnes, K.; Jacobsen, M.; Lea, T. EP receptor expression in human intestinal epithelium and localization relative to the stem cell zone of the crypts. *PLoS ONE* **2011**, *6*, e26816. [[CrossRef](#)]
22. Eberhart, C.E.; Dubois, R.N. Eicosanoids and the gastrointestinal tract. *Gastroenterology* **1995**, *109*, 285–301. [[CrossRef](#)]
23. Hoque, K.M.; Chakraborty, S.; Sheikh, I.A.; Woodward, O.M. New advances in the pathophysiology of intestinal ion transport and barrier function in diarrhea and the impact on therapy. *Expert Rev. Anti Infect. Ther.* **2012**, *10*, 687–699. [[CrossRef](#)] [[PubMed](#)]
24. Field, M. Intestinal ion transport and the pathophysiology of diarrhea. *J. Clin. Investig.* **2003**, *111*, 931–943. [[CrossRef](#)]
25. Dudeja, P.K.; Gill, R.K.; Ramaswamy, K. Absorption, secretion and epithelial cell function. In *Colonic Diseases*; Koch, T.R., Ed.; Humana Press: Totowa, NJ, USA, 2003; pp. 3–24.
26. Gill, R.K.; Alrefai, W.A.; Borthakur, A.; Dudeja, P.K. Intestinal anion absorption. In *Physiology of the GI Tract*, 5th ed.; Elsevier: Cambridge, MA, USA, 2012; pp. 1819–1848.
27. Arthur, S.; Palaniappan, B.; Mani, K.; Sundaram, U. Inducible Nitric Oxide Mediates the Inhibition of Coupled NaCl Absorption in a Mouse Model of Spontaneous Ileitis. *Gastroenterology* **2018**, *154*, S-193. [[CrossRef](#)]
28. Czuba, L.C.; Hillgren, K.M.; Swaan, P.W. Post-translational modifications of transporters. *Pharmacol. Ther.* **2018**, *192*, 88–99. [[CrossRef](#)]
29. Loo, D.D.; Zeuthen, T.; Chandy, G.; Wright, E.M. Cotransport of water by the Na⁺/glucose cotransporter. *Proc. Natl. Acad. Sci. USA* **1996**, *93*, 13367–13370. [[CrossRef](#)]
30. Binder, H.J.; Brown, I.; Ramakrishna, B.S.; Young, G.P. Oral rehydration therapy in the second decade of the twenty-first century. *Curr. Gastroenterol. Rep.* **2014**, *16*, 376. [[CrossRef](#)]
31. Nalin, D.R.; Levine, M.M.; Mata, L.; de Cespedes, C.; Vargas, W.; Lizano, C.; Loria, A.R.; Simhon, A.; Mohs, E. Comparison of sucrose with glucose in oral therapy of infant diarrhoea. *Lancet* **1978**, *2*, 277–279. [[CrossRef](#)]
32. Buccigrossi, V.; Lo Vecchio, A.; Bruzzese, E.; Russo, C.; Marano, A.; Terranova, S.; Cioffi, V.; Guarino, A. Potency of Oral Rehydration Solution in Inducing Fluid Absorption is Related to Glucose Concentration. *Sci. Rep.* **2020**, *10*, 7803. [[CrossRef](#)] [[PubMed](#)]
33. Donnellan, C.F.; Yann, L.H.; Lal, S. Nutritional management of Crohn's disease. *Therap. Adv. Gastroenterol.* **2013**, *6*, 231–242. [[CrossRef](#)]
34. Sundaram, U.; Knickelbein, R.G.; Dobbins, J.W. pH regulation in ileum: Na⁽⁺⁾-H⁺ and Cl⁽⁻⁾-HCO₃⁻ exchange in isolated crypt and villus cells. *Am. J. Physiol.* **1991**, *260 Pt 1*, G440–G449. [[CrossRef](#)]
35. Sundaram, U.; Coon, S.; Wisel, S.; West, A.B. Corticosteroids reverse the inhibition of Na-glucose cotransport in the chronically inflamed rabbit ileum. *Am. J. Physiol.* **1999**, *276*, G211–G218. [[CrossRef](#)] [[PubMed](#)]
36. Sundaram, U.; Wisel, S.; Rajendren, V.M.; West, A.B. Mechanism of inhibition of Na⁺-glucose cotransport in the chronically inflamed rabbit ileum. *Am. J. Physiol.* **1997**, *273*, G913–G919. [[CrossRef](#)] [[PubMed](#)]
37. Sundaram, U.; West, A.B. Effect of chronic inflammation on electrolyte transport in rabbit ileal villus and crypt cells. *Am. J. Physiol* **1997**, *272 Pt 1*, G732–G741. [[CrossRef](#)]
38. Palaniappan, B.; Arthur, S.; Sundaram, V.L.; Butts, M.; Sundaram, S.; Mani, K.; Singh, S.; Nepal, N.; Sundaram, U. Inhibition of intestinal villus cell Na⁺/K⁺-ATPase mediates altered glucose and NaCl absorption in obesity-associated diabetes and hypertension. *FASEB J.* **2019**, *33*, 9323–9333. [[CrossRef](#)] [[PubMed](#)]